Dynamics of a De Novo Designed Three-Helix Bundle Protein Studied by ^{15}N, ^{13}C, and ^{2}H NMR Relaxation Methods†

Scott T. R. Walsh, Andrew L. Lee,‡ William F. DeGrado, and A. Joshua Wand*

The Johnson Research Foundation and Department of Biochemistry and Biophysics, University of Pennsylvania, Philadelphia, Pennsylvania 19104-6059

Received March 14, 2001; Revised Manuscript Received June 15, 2001

ABSTRACT: Understanding how the amino acid sequence of a polypeptide chain specifies a unique, functional three-dimensional structure remains an important goal, especially in the context of the emerging discipline of de novo protein design. α_3D is a single chain protein of 73 amino acids resulting from a de novo design effort. Previous solution nuclear magnetic resonance studies of α_3D confirm that the protein adopts the designed structure of a three-helix bundle. Furthermore, α_3D has been previously shown to possess all of the major thermodynamic and structural characteristics of natural proteins, though it shares no sequence homology to any protein sequence in the database. In this work, the backbone and side-chain dynamics of α_3D were investigated using ^{15}N, ^{13}C, and ^{2}H nuclear magnetic resonance relaxation methods with the aim of assessing the character of the internal motions of this native-like protein of de novo design. At the backbone level, both ^{15}N and $^{13}C_\alpha$ relaxation studies indicate highly restrictive motion on the picosecond to nanosecond time scale in the α-helical regions of α_3D, with increasing mobility at the ends of the α-helices and in the two loop regions. This is largely consistent with what is seen in proteins of natural origin. Overall, the view provided by both ^{2}H and ^{13}C methyl relaxation methods suggest that the side chains of α_3D are more dynamic compared to natural proteins. Regions of relative flexibility bound clusters of rigid methyl-bearing side-chain groups that are interspersed with aromatic and *β*-branched amino acids. The time scale of motions associated with methyl-bearing side chains of α_3D are significantly longer than that seen in natural proteins. These results indicate that the strategies underlying the design of α_3D have largely, but not completely, captured both the structural and dynamic character of natural proteins.

The robust de novo design of conformationally specific hydrophobic cores of proteins such as those typically seen in proteins of natural origin remains a significant challenge. More often than not, proteins of de novo design have adopted structural, dynamic and thermodynamic features more characteristic of the protein molten globule than of native-state proteins (*1*). To overcome this deficiency, there has been an intense effort in the development of computational repacking algorithms that can assist in the design of protein interiors [for a review see Lazar and Handel (*2*)]. Several studies have shown the importance of including *β*-branched and aromatic residues within the hydrophobic core with the aim of restricting side-chain mobility (*3*−*6*). Recently, de novo designed coiled coils (*7*, *8*), several four-helix bundle proteins (*5*, *9*−*11*) and a three-helix bundle protein (*12*) have been shown to have native-like structure indicating that robust design principles are beginning to emerge.

Our view of the internal dynamics of natural proteins is also evolving. Extensive nuclear magnetic resonance (NMR)[1]-based studies have indicated that motion on the main chain of natural proteins is generally of high frequency and small amplitude with exceptions being restricted to loops and elements lacking classical secondary structure (e.g., refs *13*−*16*). In contrast, a theme emerging from NMR relaxation studies of methyl-bearing side chains of proteins is that the hydrophobic cores of natural proteins are quite dynamic and heterogeneously so (*17*−*23*). Most recently, it has been suggested that the subnanosecond time-scale motions of methyl-bearing side chains in native proteins tend to cluster into three distinct classes of angular order (*24*). The presence of significant dynamics brings into play the role of residual conformational entropy in stabilizing the folded state of the protein (*25*). Understanding the side-chain dynamics in the cores of natural proteins using NMR relaxation methods should reveal the principles necessary to allow for the successful design of more native-like hydrophobic cores. In this regard, similar studies of de novo designed proteins will further enrich our understanding of the detailed success of

† This work was supported by NIH Grants GM35940 and GM54616, the NSF MRSEC program (DMR00-79909) and by equipment grants from the NIH and the ARO. A.L.L is a recipient of a NIH postdoctoral fellowship. This study made use of the National Nuclear Magnetic Resonance Facility at Madison, which is supported by NIH Grants RR02301, RR02781, and RR08438, by NSF Grants DMB-8415048, BIR-9214394, the University of Wisconsin, and the U.S. Department of Agriculture.

* To whom correspondence should be addressed. Phone: (215) 573-7288. Fax: (215) 573-7290. E-mail: wand@mail.med.upenn.edu.

‡ Present address: Division of Medicinal Chemistry and Natural Products, School of Pharmacy, CB# 7360 - Beard Hall, University of North Carolina at Chapel Hill, Chapel Hill, NC 27599-7360.

[1] Abbreviations: fid, free induction decay; LRCC, long-range coupling constant; NOE, nuclear Overhauser effect; T_1, spin lattice relaxation time; T_2, spin−spin relaxation time.

10.1021/bi0105274 CCC: $20.00
Published on Web 07/21/2001

de novo protein design. α_3D is a particularly appropriate candidate for such an analysis as it has proven to be a de novo designed three-helix bundle protein having both native-like thermodynamic and structural characteristics (*12*). Here the internal dynamics of both the backbone and side chains of α_3D are investigated using ^{15}N, ^{13}C, and ^{2}H NMR relaxation methods.

EXPERIMENTAL PROCEDURES

Sample Preparation. A uniformly ^{15}N labeled α_3D sample was prepared for the ^{15}N relaxation experiments by growing BL21(DE3) *Escherichia coli* cells on $^{15}NH_4Cl$ (1 g/L, Isotec). A specifically labeled $^{13}C_\alpha$ carbon at alanine and leucine residues in α_3D was prepared by growth on amino acids supplemented with $^{13}C_\alpha$ labeled alanine and leucine (Isotec). A uniformly ^{15}N, ^{13}C, and randomly fractionally ^{2}H (50%) α_3D sample was prepared using M9 minimal media with $^{15}NH_4Cl$ (1 g/L), [U-^{13}C]glucose (2 g/L, Isotec) grown in 50% H_2O:$^{2}H_2O$. The alanine, leucine, valine, and isoleucine γ methyl groups were specifically labeled with ^{13}C by growing the cells in 0.3%-^{13}C(3)-sodium pyruvate (w/v, Cambridge) as the sole carbon source with $^{15}NH_4Cl$ in M9 minimal media as described (*26*). All samples were purified as described previously (*12*). All samples were 2 mM except the pyruvate grown sample, which was 1.7 mM. All samples were prepared in 50 mM d_3-sodium acetate (pH 5.0), 0.05% sodium azide, and 92%:8% H_2O:$^{2}H_2O$.

NMR Spectroscopy. NMR experiments were conducted using Varian Inova 500 (11.7 T), 600 (14.1 T), and 750 (17.6 T) spectrometers equipped with three-axis pulsed field gradient triple resonance probes. Also, a ^{15}N T_1 data set was collected on a Bruker DMX-400 (9.4 T) spectrometer equipped with ^{1}H/^{15}N/^{13}C/^{31}P probe and *z*-axis pulsed field gradients (at NMRFAM, University of Wisconsin, Madison, WI). The temperature was calibrated to 30.0 ± 0.5 °C using a 100% methanol sample (27).

^{15}N Relaxation Measurements. ^{15}N T_1, T_2, and {^{1}H}-^{15}N NOE experiments employed pulse sequences as described by Farrow et al. (*28*). ^{15}N T_1 experiments were carried out at 9.4, 11.7, and 14.1 T. At 9.4 T, the ^{15}N T_1 relaxation delays were 30*, 50, 80, 120*, 170.0, 220.0, 290.0, 350.0, 430.0*, 510.0, 600.0, and 700.0 ms. Asterisks indicate duplicated measurements. At 11.7 T, ^{15}N T_1 delay periods were 55, 90*, 125, 195.0, 275.0*, 355.0, 445.0, 545.0, 655.0, 755.0*, 850.0, and 1005.0 ms. At 14.1 T, ^{15}N T_1 delay periods were 54*, 84, 114.0, 164.0*, 234.0, 314.0, 424.0, 544.0*, 684.0, 844.0, 1014.0, and 1214.0 ms. ^{15}N T_2 experiments were carried out at 11.7 and 14.1 T with a CPMG pulse train of 12.6*, 24.6, 47.6, 72.6, 83.6*, 100.6, 114.6*, 126.6, 141.6, and 153.6 ms with a 5.1 kHz field strength, and 9.0*, 34.0, 59.0*, 84.0, 109.0, 134.0*, and 160.0 ms with a 6.25 kHz field strength, respectively. ^{15}N T_1 and T_2 experiments were run with 8−24 transients/fid and with a total recycle delay of 1.1−1.5 s. In the {^{1}H}-^{15}N NOE experiments, a steady state was reached after at least 3 s of 120° ^{1}H saturation pulses placed every 5 ms, and a total recycle of 5 s was used to allow for the longitudinal ^{15}N magnetization to reach equilibrium. Spectra with and without the NOE were collected in an interleaved manner. For all experiments, the ^{15}N carrier was positioned at 116 ppm with a typical spectral width of 33 ppm, while the ^{1}H carrier was placed on H_2O with a spectral width of ~12 ppm. Experiments were collected with 1024 (^{1}H) by 120−160 (^{15}N) complex points.

^{13}C α Relaxation Measurements. $^{13}C_\alpha$ T_1, T_2, and {^{1}H}-$^{13}C_\alpha$ NOE experiments were carried as described (*28*) adapted for the methine carbon. At 11.7 T, $^{13}C_\alpha$ T_1 relaxation delays were 80.5*, 115.5, 150.5, 220.5, 300.5, 380.5*, 470.5, 570.5, 685.0, 780.5*, 910.5, and 1030.5 ms with 16 transients/fid. $^{13}C_\alpha$ T_2 experiments consisted of a CPMG pulse trains of 11.4*, 20.4, 27.4, 36.4*, 43.4, 51.4, 66.4, 82.4*, 98.4, and 114.4 ms with a 20.0 kHz field strength and 16 transients/fid. The {^{1}H}-$^{13}C_\alpha$ NOE experiment was collected in a similar manner as described for the {^{1}H}-^{15}N NOE experiment, with 44 transients/fid. For all the $^{13}C_\alpha$ experiments the ^{13}C carrier was positioned at 52.5 ppm with a spectral width of 10 ppm, and the ^{1}H carrier was placed on H_2O with a spectral width of 13 ppm. Experiments were collected with 1024 (^{1}H) by 120 (^{13}C) complex points.

^{2}H Methyl Relaxation Measurements. Measurements for multiple spin coherence involving deuterium were measured for $R(I_zC_z)$, $R(I_zC_zD_z)$, and $R(I_zC_zD_y)$ at 11.7 and 14.1 T. The pulse sequences used involved the increased resolution experiments developed by Kay and co-workers (*29*). At 11.7 T, relaxation delays were 11.0*, 18.4, 25.7, 33.1*, 40.5, 47.9, 55.2, 62.1*, and 70.0 ms for the I_zC_z; 2.2*, 6.3, 11.5, 17.7*, 24.7, 32.5, 50.0*, 59.7, and 70.0 ms for the $I_zC_zD_z$; and 1.0*, 2.7, 4.9*, 10.6, 14.0*, 17.6, 21.5, 25.6*, and 30.0 ms for the $I_zD_zD_y$. Recycle delays of 1.6, 1.8, and 2.1 s and 32, 48, and 48 transients/fid were collected for the I_zC_z, $I_zC_zD_z$, and $I_zC_zD_y$, respectively. The spectra were collected with 1024 (^{1}H) by 56 (^{13}C) complex points. At 14.1 T, relaxation delays were 2.0*, 9.4, 16.7, 24.1*, 31.5, 38.9, 46.2, 53.6*, and 61.0 ms for the I_zC_z; 2.2*, 6.3, 11.5, 17.7*, 24.7, 32.5, 40.9, 50.0*, 59.7, and 70.0 ms for the $I_zC_zD_z$; 1.0*, 2.7, 4.9*, 7.6, 10.6, 14.0*, 17.6, 21.5, 25.6*, and 30.0 ms for the $I_zD_zD_y$. Recycle delays of 2.1, 2.1, and 2.3 s and 24, 32, and 32 transients/fid were collected for the I_zC_z, $I_zC_zD_z$, and $I_zC_zD_y$, respectively. The spectra were collected with 1024 (^{1}H) by 68 (^{13}C) complex points. The ^{13}C carrier was placed at 20 ppm with a spectral width of 16 ppm, and the ^{1}H carrier was placed on H_2O with a spectral width of 12−13 ppm.

^{13}C Methyl Relaxation Measurements. ^{13}C methyl T_1 and {^{1}H}-^{13}C methyl NOE experiments were collected at 11.7, 14.1, and 17.6 T as described (*21*) with the exception at 17.6 T, at which the T_1 experiment incorporated the WATERGATE sequence (*30*). for H_2O suppression. At 11.7 T, ^{13}C methyl T_1 relaxation delays were 40.5*, 100.5, 190.5, 300.5*, 420.5, 550.5, 690.5*, 840.5, and 1005.0 ms. Enhancement from the NOE was developed for 2.3 s and the total recycle delay was 3.0 s. The spectrum was collected with 1024 (^{1}H) by 120 (^{13}C) complex points with 8 transients/fid. At 14.1 T, ^{13}C methyl T_1 relaxation delays were set to 48.5*, 120.5, 228.5, 360.5*, 504.5, 660.5, 828.5*, 1010.5, and 1205.0 ms. Enhancement from the NOE was developed for 2.3 s and the total recycle delay was 3.0 s. The spectrum was collected with 1024 (^{1}H) by 110 (^{13}C) complex points with 8 transients/fid. At 17.6 T, ^{13}C methyl T_1 relaxation delays were set to 45.0*, 125.5, 231.5, 355.5*, 496.5, 652.5, 822.5*, 1005.5, and 1205.0 ms. Enhancement from the NOE was developed for 2.5 s and the total recycle delay was 3.3 s. The spectrum was collected with 1024 (^{1}H) by 100 (^{13}C) complex points with 8 transients/fid. {^{1}H}-^{13}C methyl NOE experiments were collected with a reference experiment without ^{1}H saturation

and with ^{1}H saturation for approximately 10 T_1 values (6, 7, and 7 s for the 11.7, 14.1, and 17.6 T, respectively) in an interleaved manner. At 11.7, 14.1, and 17.6 T, the {^{1}H}-^{13}C methyl NOE spectra were collected with 12, 16, and 12 transients/fid, respectively. The ^{13}C carrier in all spectra was placed at 20.0 ppm with a spectral width of 16 ppm and the ^{1}H carrier was placed on H_2O with a spectral width of 12−14 ppm.

Data Analysis. The ^{15}N and $^{13}C_\alpha$ data set were processed into 1024 (^{1}H) by 1024 (^{15}N, ^{13}C) point matrixes and the ^{13}C methyl and ^{2}H data were processed into 1024 by 512 (^{13}C) point matrixes using the program Felix (Biosym Technologies). Cross-peak intensities were extracted and fit to a two-parameter exponential fit using the Levenberg−Marquardt algorithm (*31*). The χ^2 residuals were less than the number of measurements taken, signaly a reasonable "goodness of fit". Uncertainty in the measurements was determined from duplicate experiments for the T_1 and T_2 measurements. The steady-state NOE values were determined from the intensity of the NOE divided by the reference experiment. The error was estimated from the root-mean-square of the baseline noise, and to be conservative, this value was doubled. Typical errors in the ^{15}N, $^{13}C_\alpha$, ^{13}C methyl, and ^{2}H relaxation parameters ranged from 1 to 4%. A duplicate {^{1}H}-^{13}C methyl NOE experiment was collected at 17.1 T, and the error was approximately 1%.

Characterization of Global and Local Motion. The anisotropy of global tumbling was assessed using the "local site approach" implemented in the programs Quadric 1.1 program (*32*) and an in-house program (*33*) The simple (*34*, *35*) and extended (*36*) model-free spectral densities were used as described below. Model-free internal dynamic parameters were determined using the local site treatment, using a nonlinear least-squares Powell minimization (*31*) as described previously (*21*, *33*). Parameter errors were estimated from 150 Monte Carlo simulations. The ^{15}N and ^{13}C chemical shift anisotropy ($\Delta\sigma$) was fixed at −170 (*33*, *37*, *38*) and 25 ppm (*39*), respectively. The bond lengths used for the N−H of 1.02 Å, C_α-H of 1.095 Å (*40*), and C methyl-H of 1.115 Å (*40*). The quadrupolar coupling constant (e^2qQ/h) of 165 kHz (*41*) was used for the ^{2}H methyl analysis.

Determination of Side-Chain Coupling Constants. The χ^1 angles for the isoleucine, valine, and threonine residues were calculated from $^3J_{NC\gamma}$ and $^3J_{COC\gamma}$ coupling constants obtained from quantitative *J*-correlation experiments (*42*, *43*). The χ^2 angles of leucine and isoleucine residues were calculated from $^3J_{C\delta C\alpha}$ coupling constants obtained from a three-dimensional long-range carbon coupling (LRCC) experiment (*44*). The LRCC pulse sequence was modified from the original experiment to include continuous SEDUCE−1 carbonyl decoupling during t_1 and t_2 evolution periods and included a WATERGATE sequence for water suppression (*30*).

RESULTS

Characterization of Global Tumbling. A critical first step in the analysis of NMR relaxation data obtained on macromolecules is the assessment of the degree of anisotropy of molecular reorientation. Analysis of the lowest energy solution structure of α_3D reveals principal moments of interia of 1.00:0.94:0.34, suggesting the possibility of significant anisotropy of tumbling in solution. This was addressed by analysis of obtained ^{15}N relaxation data using the "local site approach" implemented in the programs Quadric 1.1 program (*32*) and an in-house program (*33*). ^{15}N T_1 relaxation data were collected at field strengths of 9.4, 11.7, and 14.1 T and ^{15}N T_2 and NOE data were collected at 11.7 and 14.1 T, for a total of seven data sets. The rotational correlation time (τ_m) of α_3D was determined using a reduced set of ^{15}N sites. Sites were excluded if the obtained ^{15}N NOE value was less than 0.60, if there was an unanticipated field dependence of the ^{15}N T_2 measurements, indicating contamination by chemical exchange processes (R_{ex}), or if the cross-peak was ill-resolved. These criteria resulted in a set of 35 of 73 residues being used to characterize global tumbling. Using these data, the solution structure of α_3D was fit to isotropic, axially symmetric, and a fully anisotropic models. The global effective correlation time ($\tau_{m,eff}$) was determined as $\tau_{m,eff} - 1 = 6D_{eff}$, where D_{eff} is the sum of the diagonal components from the diffusion tensor ($D_{eff} = {}^1/_3(D_{xx} + D_{yy} + D_{zz})$ (*32*). The best fits obtained for α_3D are to an axially symmetric diffusion tensor. Using only the ^{15}N T_1 and NOE data, the $D_\parallel/D_\perp$ is 1.48 ± 0.14 with a $\tau_{m,eff}$ of 6.54 ns compared to the value of 5.20 ns determined from the isotropic model. Anisotropic fits are too demanding when only using T_1 and NOE data. Incorporation of the ^{15}N T_2 data, however, shows a dramatic smoothing in the fitting of the diffusion tensor due to the J(0) information from the ^{15}N T_2. The $D_\parallel/D_\perp$ is 1.26 ± 0.06 and an $\tau_{m,eff}$ of 5.59 ns similar to the value of 5.50 ns determined for the isotropic model. Incorporation of the $^{13}C_\alpha$ data set, yields $D_\parallel/D_\perp$ value of 0.57 ± 0.03. Similar behavior has been seen for ubiquitin (*33*) and cytochrome c_2 (*45*) exhibiting two minima corresponding to prolate and oblate shapes. The $\tau_{m,eff}$ from the ^{15}N (T_1, T_2, and NOE) and $^{13}C_\alpha$ (T_1, T_2, and NOE) data yields a value of 5.16 ns very similar to the value of 5.20 ns determined using only ^{15}N T_1 and NOE data fit to an isotropic model. In summary, using the ^{15}N T_1 and NOE data, an isotropic τ_m of 5.2 ns was obtained and inflates to 5.5 ns when T_2 are included, similar to what has been seen previously (*33*). Finally, calculations of the simple model-free squared generalized order parameters (S^2) and the effective correlation times (τ_e) using an axially symmetric diffusion tensor yield values within experimental error of those derived from the isotropic model.

Backbone Dynamics. Simple model-free parameters obtained for the backbone N−H bonds of α_3D are shown on a per residue basis in Figure 1. They are similar to those seen for natural proteins in regions of secondary structure, with S^2 values ranging from 0.80 to 0.85. As with natural proteins, the N−H S^2 values decrease at the ends of the α-helices and in the two loop regions. The effective correlation times (τ_e) average 45 ps in the α-helices to 150 ps in the more flexible regions of α_3D, again typical values for a natural protein.

The W4 indole N−H is resolved in the ^{15}N−HSQC spectrum, which allows for determination of its relaxation parameters. The indole N−H has a S^2 value of 0.61 (using a CSA of −170 ppm) while the backbone N−H of W4 has a S^2 value of 0.74. The solution structure of α_3D shows that the indole N−H bond points toward solvent (*12*). Using a probe sphere radius of 1.4 Å, the W4 side chain is 34% solvent exposed. The indole N−H has similar mobility to

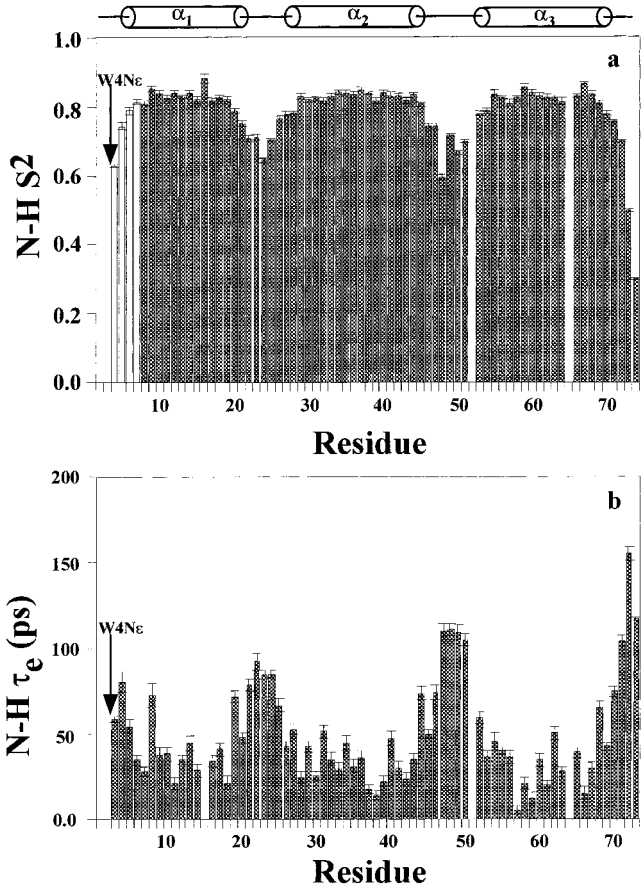

FIGURE 1: (a) ^{15}N-derived amide N−H squared generalized order parameters determined for α_3D using ^{15}N T_1 (9.4, 11.7, and 14.1 T) and NOE (11.7 and 14.1 T) data at 30 °C. (b) The corresponding effective correlation times, τ_e. An isotropic rotational correlation time (τ_m) of 5.2 ns was used.

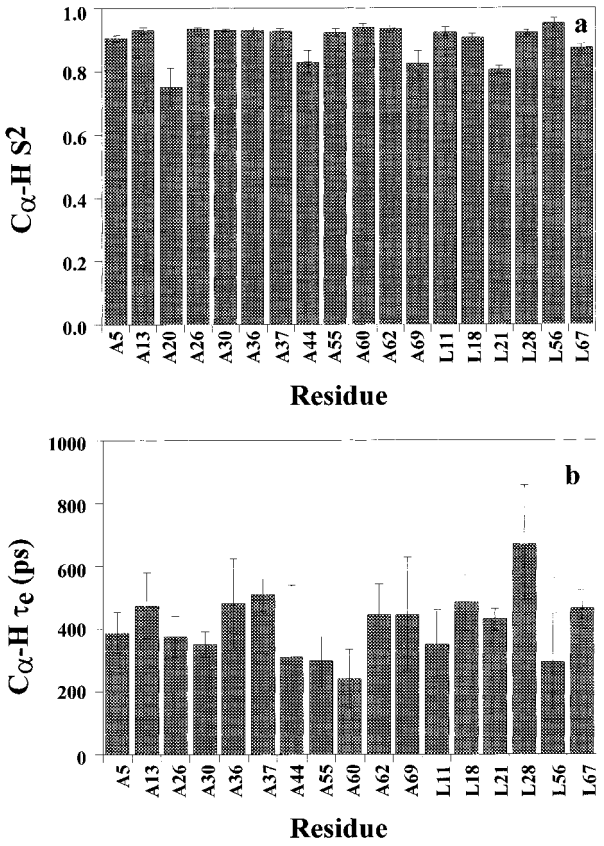

FIGURE 2: (a) ^{13}C-derived α C−H squared generalized order parameters determined for alanine and leucine residues of α_3D at 30 °C. (b) The corresponding effective correlation times, τ_e. A12, A29, and A61 were not determined due to spectral overlap. An isotropic correlation time (τ_m) of 5.2 ns was used.

the two loop regions (G22−G23 and K46−P51) of α_3D (Figure 1).

The dynamics of the polypeptide backbone were also studied using $^{13}C_\alpha$ relaxation of alanine and leucine residues. T_1, T_2, and NOE experiments were carried out in 92:8% H_2O:^2H_2O at 11.7 T, to match solution conditions to the ^{15}N sample. The experiments were implemented in identical fashion to the ^{15}N-based experiments, using gradient coherence selection as an effective method of water suppression (*28*). There are 15 alanine and 7 leucine residues in α_3D. Twelve of the 15 alanine residues were sufficiently resolved to allow accurate quantification of the relaxation parameters. $^{13}C_\alpha$-H S^2 and τ_e values were determined for six of seven leucine residues (L42 did not yield a unique solution). Figure 2 shows the obtained C_α-H S^2 and τ_e values. The uniformly high C_α-H S^2 values (∼0.90) are indicative of extremely restricted motion of the C_α-H vectors in the ps-ns time regime. The relatively low C_α-H S^2 values of alanine and leucine residues are in close proximity to the loop regions (A20, L21, and A44) and the C-terminus (L67 and A69). The $^{13}C_\alpha$-H S^2 values are higher than the corresponding N−H S^2 value by ∼0.10. Similar behavior has been seen for ^{15}N- and ^{13}C-relaxation studies of cyclosporin A (*46*), ubiquitin (*14*, *18*) and the snake toxin α from *Naja nigricollis* (*47*, *48*). Molecular dynamics simulations suggest that this behavior can result from anti-correlated fluctuations of the torsion angles of Ψ_{i-1} and Φ_i (*48*, *49*). The $^{13}C_\alpha$ τ_e times average 400 ps, which is approximately 100 ps longer than the average of 300 ps determined for ubiquitin (*18*).

Side-Chain Dynamics. Deuterium T_1 and $T_{1\rho}$ relaxation times were determined at 11.7 and 14.1 T for the majority of methyl groups of α_3D. Exceptions include alanine β methyl groups where the ^{1}H-^{13}C methyl correlations were not sufficiently resolved. The δ methyl groups of L11, L18, and L21 have minor resonance overlap and therefore their relaxation parameters should be interpreted with caution. The symmetry axis squared generalized order parameters (S_{axis}^2) and the corresponding effective correlation times are listed in Table 1 and illustrated in Figures 3 and 4. Also provided in Table 1 are the corresponding effective cone angles derived from the "diffusion in a cone" model (*34*, *35*) using the following equation:

$$\theta = \cos^{-1}\left[\frac{1}{2}((1 + 8S_{axis}^2)^{\frac{1}{2}} - 1)\right] \qquad (1)$$

The S_{axis}^2 values of the methyl groups of α_3D are on average *lower* than the average S_{axis}^2 values determined for natural proteins (*22*). The alanine β methyl groups have S_{axis}^2 values ranging from 0.57 to 0.79. They have an average S_{axis}^2 value of 0.64, which is approximately 0.20 lower than that seen in natural proteins (*22*). A60$^\beta$ has the highest S_{axis}^2 value of 0.79, which correlates well with this side chain being buried in the hydrophobic core. Interestingly, the S_{axis}^2 values for A20$^\beta$, A26$^\beta$, and A44$^\beta$ are significantly different and lower (Table 1) than their corresponding C_α-H S^2 values (Figure

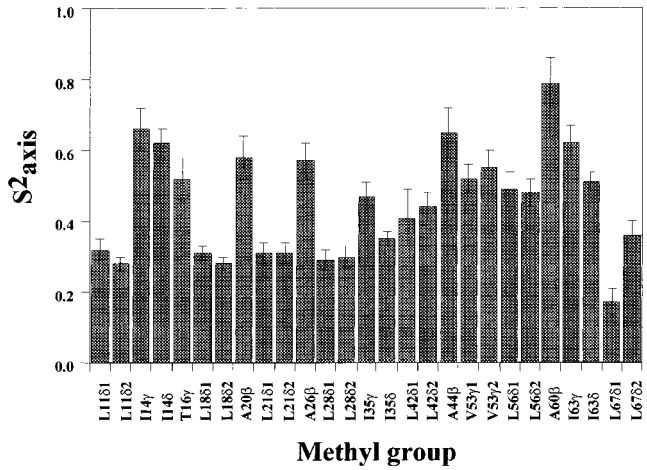

FIGURE 3: ^{2}H-derived methyl symmetry axis squared generalized order parameters (S_{axis}^2) determined for α_3D at 30 °C.

Table 1: α_3D Methyl Simple Model-Free (SMF) Parameters from the ^{2}H Relaxation at 30 °C

	S_{axis}^2	τ_e (ps)	χ_{M-n}^2	θ (deg)
L11$^{\delta1}$	0.32 ± 0.03	49.9 ± 1.8	5.0	47.6
L11$^{\delta2}$	0.28 ± 0.02	53.9 ± 2.1	0.1	50.0
I14$^{\gamma}$	0.66 ± 0.06	38.1 ± 4.0	0.4	29.6
I14$^{\delta}$	0.62 ± 0.04	18.8 ± 2.2	0.0	31.9
T16$^{\gamma}$	0.52 ± 0.06	59.9 ± 2.5	2.4	36.7
L18$^{\delta1}$	0.31 ± 0.02	51.5 ± 1.9	0.1	48.4
L18$^{\delta2}$	0.28 ± 0.02	54.2 ± 2.1	0.6	50.1
A20$^{\beta}$	0.58 ± 0.06	44.6 ± 2.8	0.5	33.8
L21$^{\delta1}$	0.31 ± 0.03	53.1 ± 2.0	0.6	48.0
L21$^{\delta2}$	0.31 ± 0.03	51.7 ± 3.6	6.5	48.1
A26$^{\beta}$	0.57 ± 0.05	46.8 ± 2.4	0.1	34.1
L28$^{\delta1}$	0.29 ± 0.03	60.6 ± 2.4	0.3	49.2
L28$^{\delta2}$	0.30 ± 0.03	58.1 ± 1.9	0.7	49.0
I35$^{\gamma}$	0.47 ± 0.04	55.0 ± 2.1	1.5	39.1
I35$^{\delta}$	0.35 ± 0.02	30.0 ± 1.9	0.9	45.8
L42$^{\delta1}$	0.41 ± 0.08	57.7 ± 7.2	0.1	42.8
L42$^{\delta2}$	0.44 ± 0.04	55.7 ± 2.5	0.1	41.0
A44$^{\beta}$	0.65 ± 0.07	43.1 ± 3.0	0.4	30.2
V53$^{\gamma1}$	0.52 ± 0.04	50.8 ± 2.0	0.3	36.9
V53$^{\gamma2}$	0.55 ± 0.05	49.4 ± 2.3	0.3	35.3
L56$^{\delta1}$	0.49 ± 0.05	53.9 ± 4.8	0.3	38.4
L56$^{\delta2}$	0.48 ± 0.04	43.2 ± 3.2	0.2	39.0
A60$^{\beta}$	0.79 ± 0.07	41.2 ± 2.3	0.3	22.6
I63$^{\gamma}$	0.62 ± 0.05	39.9 ± 3.6	0.2	31.7
I63$^{\delta}$	0.51 ± 0.03	27.0 ± 2.1	0.5	37.4
L67$^{\delta1}$	0.17 ± 0.04	75.0 ± 6.0	3.2	57.7
L67$^{\delta2}$	0.36 ± 0.04	56.1 ± 2.5	0.7	45.4

2). This indicates that the $C_\alpha C_\beta$ vector is not collinear with the effective director axis of the motion.

The leucine δ methyl groups of α_3D also display a greater amplitude of motion than in natural proteins, with an average difference of approximately 0.12 [$\langle S_{axis}^2\rangle$ of 0.32 for α_3D versus $\langle S_{axis}^2\rangle$ of 0.44 for natural proteins (*22*)]. The obtained S_{axis}^2 values for each of the methyl groups of each leucine residue agree well with each other except for L67 (δ^1 of 0.17 and δ^2 of 0.36, Table 1). Thus, in nearly all cases, the effective director of the motion appears to lie in a plane that bisects the $C_\gamma-C_\delta$ vectors, i.e., director axis projects equal components onto both symmetry axes. The L67$^{\delta1}$ methyl group has the largest amplitude of motion, having a S_{axis}^2 value of 0.17, corresponding to a free diffusion cone angle of ~58° (Table 1). The γ methyl groups of the three isoleucine residues (I14, I35, I63) have an average S_{axis}^2 value of 0.57. This is about 0.20 lower than that seen in natural

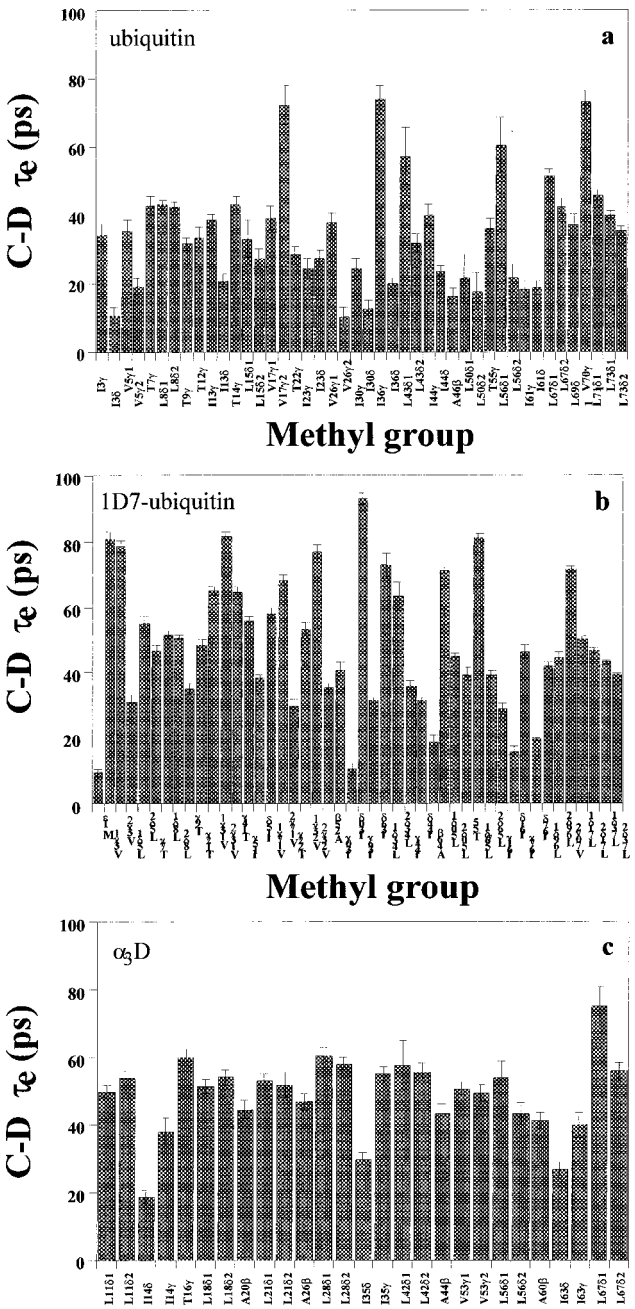

FIGURE 4: (a) Effective correlation times (τ_e) determined from the ^{2}H methyl analysis fit to the simple model-free formalism (SMF, eq 8) for ubiquitin at 30 °C (*21*). (b) The τ_e times determined from the ^{2}H methyl analysis for a repacked ubiquitin variant, 1D7, at 30 °C (*50, 51*). (c) The τ_e times determined from the ^{2}H methyl analysis for α_3D at 30 °C.

proteins (*21*−*23*). On the other hand, the average S_{axis}^2 value of 0.47 seen for the δ methyls of isoleucines in α_3D is similar to that observed in natural proteins (*21*, *22*). The ^{2}H-derived effective correlation times (τ_e) of the methyl groups of α_3D range from 18.8 to 75.0 ps, with an average value of 47.7 ps (Table 1).

Notwithstanding the inherent limitations of ^{2}H-derived τ_e values (*21*), the distribution of τ_e times of methyl groups in ubiquitin (*21*), a repacked ubiquitin variant, 1D7 (*50, 51*) and in α_3D show a similarly broad distribution (Figure 4). The results obtained for α_3d were sufficiently compelling for us to undertake a more exhaustive study using carbon

Table 2: α_3D Methyl Model-Free Parameters from the ^{13}C Methyl Relaxation at 30 °C

	S_{axis}^2	τ_e (ps)	χ_{M-n}^2	S_{axis}^2	τ_f (ps)	τ_{axis} (ps)	χ_{M-n}^2
L11$^{\delta1}$	1.39 ± 0.04	26.2 ± 0.3	1.8		24.3 ± 0.5		1.2
L11$^{\delta2}$	1.15 ± 0.05	35.1 ± 0.3	5.1	0.76 ± 0.08	32.2 ± 1.1	674 ± 261	2.0
I14$^{\gamma}$	1.19 ± 0.04	23.0 ± 0.2	1.2		21.4 ± 0.7		0.1
L18$^{\delta1}$	1.39 ± 0.04	30.8 ± 0.3	13.7	0.50 ± 0.08	25.4 ± 0.9	584 ± 90	1.1
L18$^{\delta2}$	1.24 ± 0.04	32.5 ± 0.3	17.6	0.55 ± 0.08	27.2 ± 0.9	500 ± 59	3.9
A20$^{\beta}$	1.28 ± 0.04	23.2 ± 0.3	5.58		22.7 ± 1.2		1.8
L21$^{\delta1}$	1.13 ± 0.04	34.3 ± 0.3	15.2	0.85 ± 0.04	32.6 ± 0.6	979 ± 266	8.8
L21$^{\delta2}$	1.28 ± 0.03	28.5 ± 0.2	13.2	0.57 ± 0.07	23.9 ± 0.1	513 ± 68	1.3
A26$^{\beta}$	1.20 ± 0.05	35.0 ± 0.3	33.5		33.8 ± 0.6		22.2
L28$^{\delta1}$	3.30 ± 0.10	55.8 ± 1.0	7.0		35.0 ± 1.2	1980 ± 536	1.3
L28$^{\delta2}$	2.97 ± 0.08	43.4 ± 0.7	8.0		29.1 ± 0.1	1730 ± 369	0.5
I35$^{\gamma}$	1.58 ± 0.04	28.4 ± 0.3	15.8	0.55 ± 0.10	25.0 ± 0.1		7.7
L42$^{\delta1}$	1.45 ± 0.04	32.7 ± 0.3	8.1	0.61 ± 0.04	28.8 ± 0.7	967 ± 231	1.2
L42$^{\delta2}$	1.51 ± 0.05	33.4 ± 0.3	2.6		30.6 ± 0.1		1.2
A44$^{\beta}$	1.28 ± 0.04	26.4 ± 0.3	1.1		25.4 ± 0.4		0.8
V53$^{\gamma1}$	1.29 ± 0.04	30.8 ± 0.3	2.8		29.6 ± 0.4		1.9
V53$^{\gamma2}$	1.27 ± 0.05	32.8 ± 0.3	1.9		31.5 ± 0.5		1.3
L56$^{\delta1}$	1.46 ± 0.05	40.7 ± 0.4	3.4	0.63 ± 0.12	36.8 ± 0.8		0.5
L56$^{\delta2}$	1.13 ± 0.03	26.6 ± 0.2	2.0		25.5 ± 0.5		0.7
A60$^{\beta}$	1.42 ± 0.02	31.2 ± 0.2	5.6		29.4 ± 0.3		3.8
I63$^{\gamma}$	1.04 ± 0.03	23.8 ± 0.2	1.5		24.7 ± 1.5		0.6
L67$^{\delta1}$	1.61 ± 0.05	45.7 ± 0.4	5.6		40.5 ± 0.7		2.0
L67$^{\delta2}$	1.62 ± 0.04	34.6 ± 0.3	7.4	0.51 ± 0.05	29.8 ± 0.8	1060 ± 283	0.5

relaxation methods. To obtain better estimates of the time scales of the methyl group dynamics (*21*), the ^{13}C methyl T_1 and NOE values were measured for α_3D at field strengths of 11.7, 14.1, and 17.6 T. An α_3D sample was prepared by expressing the protein using ^{13}C methyl labeled pyruvate as described (*26*). This method specifically labels with ^{13}C only the methyl groups of leucine δs, valine γs, isoleucine γs, and alanine βs (~90%), and thus removes complications from ^{13}C−^{13}C coupling (*26*). For reasons outlined previously (*21*), the extended model-free treatment is used to analyze the methyl carbon relaxation data. In this treatment, S^2_f is defined by the geometry of the methyl group leaving S_{axis}^2, τ_f, and τ_{axis} to be fit. The experimental fits of the relaxation parameters to the SMF and EMF models are listed in Table 2. The obtained "fast" effective correlation times (τ_f) range from 21 to 41 ps with an average value of 29 ps (Table 2). The average τ_f value for α_3D corresponds reasonably well to the value (24 ps) determined for ubiquitin (*21*). Only nine slow time scale motions (τ_{axis}) could be satisfactorily determined for α_3D using the EMF model (Table 2). Since τ_{axis} and S_{axis}^2 are linked parameters, and if τ_{axis} is long (e.g., $\tau_{axis} > 700$ ps), numerical simulations show that it is difficult to fit S_{axis}^2 confidently using only ^{13}C methyl T_1 and NOE data at current field strengths (*21*). The obtained τ_{axis} values are indeed long, with a few approaching the rotational correlation time (τ_m) of ~5 ns (Table 2). The average τ_{axis} value of ~900 ps for α_3D is about three times longer than the average τ_{axis} value of ~300 ps for ubiquitin (*21*). Interestingly, the ^{13}C τ_f times of α_3D have a more uniform profile with a standard deviation of ~5 ps (Figure 5), analogous to the methionine methyl groups in the uncomplexed state of calmodulin (*23*). Figure 6 shows the distribution of the ^{13}C τ_f values for ubiquitin and α_3D. The center of the distribution of ubiquitin (*21*) for the ^{13}C τ_f values (methyl rotation rates) lies between 10 and 20 ps, whereas the center of the distribution for α_3D is centered at 20−30 ps (Figure 6). In summary, the methyl bearing side chains of α_3D appear to have significantly larger amplitude and slower motions than observed for natural proteins of similar size.

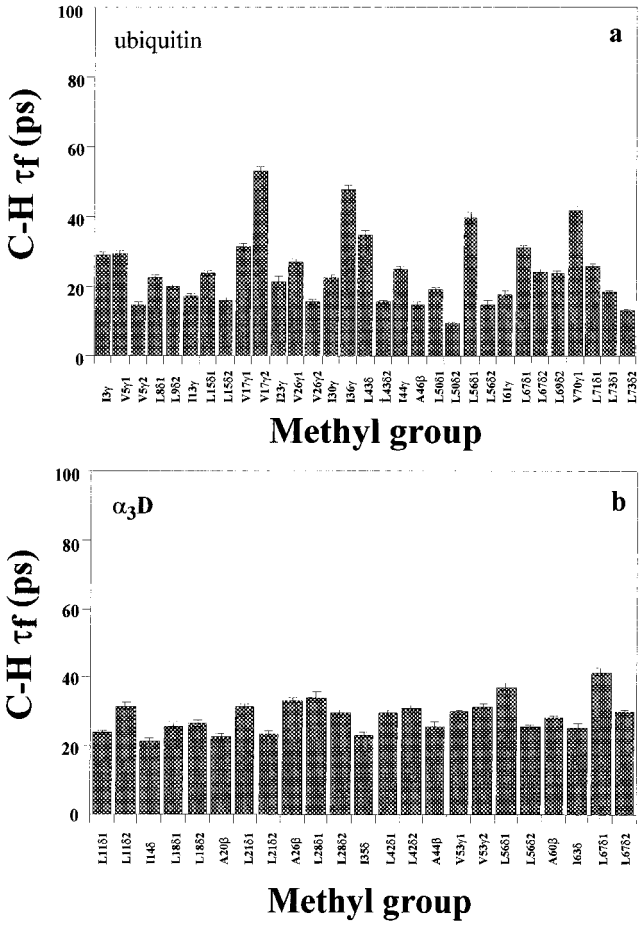

FIGURE 5: (a) Fast time scale motion (τ_f) times determined from the ^{13}C analysis fit to the extended model-free formalism (EMF, eq 9) for ubiquitin (*21*). (b) The τ_f times from the ^{13}C methyl analysis fit to the EMF for α_3D (Table 2). The τ_f parameter is interpreted as the methyl rotation rate (*21*).

Previous reports suggest that extensive deuteration results in a destabilization of native proteins (*52*). A thermodynamic

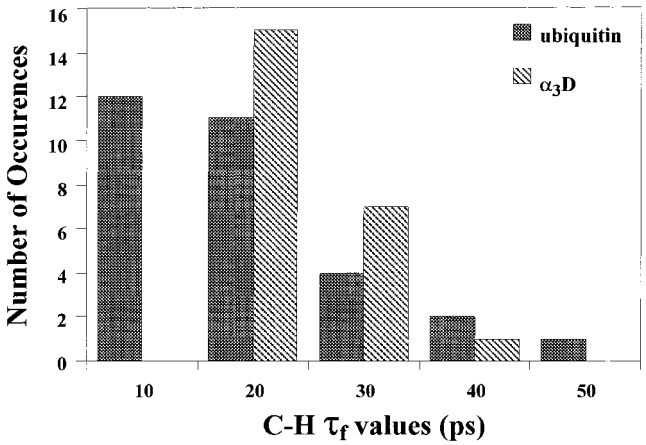

FIGURE 6: Histogram of the distribution of ^{13}C-derived τ_f values for methyl groups of ubiquitin (*21*) and α_3D (see Table 2).

analysis was therefore conducted on the 50% deuterated α_3D protein. The linear extrapolation method of guanidine hydrochloride denaturation indicates that the 50% deuterated α_3D is destabilized by ~1.0 kcal mol^{-1}relative to fully protonated α_3D. Furthermore, the cooperatively of unfolding (2.08 kcal mol^{-1} M^{-1}) is less than the fully protonated α_3D (2.41 kcal mol^{-1} M^{-1}), and the thermal denaturation midpoint (T_m) of the 50% deuterated α_3D is 5 °C lower than the fully protonated form of α_3D. This suggests that the presence of a 50% mixture of deuterons and hydrogens in α_3D is destabilizing and, in principle, could be also manifested in the internal dynamics of the protein.

DISCUSSION

^{2}H and ^{13}C methyl relaxation studies offer complementary information about the dynamics of methyl groups (*21*). Although there is good agreement between fast time scale parameters (^{13}C-derived τ_f and ^{2}H-derived τ_e), the corresponding S_{axis}^2 parameters do not correlate well. An in depth discussion of the potential reasons why ^{2}H and ^{13}C methyl analysis may differ is provided elsewhere (*21*). Briefly, ^{2}H methyl relaxation is useful for the determination of the S_{axis}^2 parameter due to the inherently low sampling frequencies of the deuteron. For example, at 14.1 T, frequencies of 0, 92, and 184 MHz are sampled, which puts most motions in the extreme narrowing limit ($\omega\tau \ll 1$). On the other hand, ^{13}C methyl relaxation is useful for determining the time scales of methyl dynamics due to the breadth of sampling frequencies. For example at 14.1 T, frequencies of 150, 450, 600, and 750 MHz are sampled. If the slow time scale motion (τ_{axis}) is in the approximate range of 150 ps $\leq \tau_{axis} \leq$ 800 ps at 14.1 T, than accurate determination of the S_{axis}^2 parameter compared may be achieved with ^{13}C relaxation at currently available field strengths.

Time Scale of the Methyl Group Dynamics. The time scale of methyl rotation and of motion of the methyl symmetry axis provides a unique insight into the local environments of side chains. Recent studies of natural proteins such as ubiquitin (*21*) reveal that methyl groups of interior (i.e., packed) side chains show a range of τ_e values while methyl groups of exterior (i.e., solvent accessible) side chains show a tighter and more uniform distribution of τ_e values. The methionine methyl groups in calmodulin perhaps most vividly exemplify this. In the uncomplexed form of calmodulin, the methionines are located on the surface of the protein and have a uniform profile of τ_e values (*23*). Upon binding to the calmodulin binding domain of the smooth muscle myosin light chain kinase peptide, the ^{2}H τ_e times of the methionine methyl groups adopt a significantly broader range of values, characteristic of the individual methyl groups undergoing a conformational change from being solvent exposed to a more ordered locally distinct environment (*23*).

The narrowness of the distribution of the time scales of methyl dynamics in α_3D may indicate that the local environments around the methyl groups of α_3D are not locked down in structurally unique environments in the picosecond to nanosecond time regime, in a manner observed in natural proteins. Moreover, taken together with the low S_{axis}^2 value, the substantially long τ_{axis} times (Tables 2) appear to be reporting higher amplitude, slower frequency motions (~0.5−1 ns) relative to natural proteins. This behavior would have been overlooked without the ^{13}C methyl analysis.

Structural Correlates of S_{axis}^2 Values. The mapping of S_{axis}^2 values determined from the ^{2}H analysis onto the α_3D structure shows characteristics that have been seen in natural proteins as well as features that appear unique to α_3D (Figure 7). As in natural proteins, there is heterogeneity and a significant range of S_{axis}^2 values of the methyl groups throughout the hydrophobic core of α_3D, indicating substantial motion on the ps-ns time scale (Figure 7). However, unlike natural proteins studied to date, there appears to be recognizable clustering of rigid and fluid methyl groups (Figure 7). At the N-terminal end of α_3D, there is a relatively rigid region involving the methyl groups of L42, V53, and L56 (Figure 7). The $^3J_{\alpha\beta}$, $^3J_{N\beta}$, $^3J_{NC\gamma}$, and $^3J_{COC\gamma}$ coupling constants, and ^{1}H-^{1}H NOEs indicate the preferred χ^1 angle for an α-helix of 180° for V53 (*53*). Leu56 has χ^1 ($^3J_{\alpha\beta}$, $^3J_{N\beta}$ coupling constants, and ^{1}H-^{1}H NOEs) and χ^2 ($^3J_{C\delta C\alpha}$ coupling constants) angles of −60° and 60°, respectively. The δ methyl groups of L56 also have the highest leucine S_{axis}^2 values in α_3D. Leu56 packs next to a cluster of several aromatic residues: W4, F7, and Y45. Interestingly, L42 has a χ^1 ($^3J_{\alpha\beta}$, $^3J_{N\beta}$ coupling constants, and ^{1}H-^{1}H NOEs) angle of −60°, but the χ^2 ($^3J_{C\delta C\alpha}$ coupling constants) angle undergoes rotamer averaging, yet still has the second highest leucine S_{axis}^2 value. The packing of the aromatic groups may help reduce the motions of L42, V53, and L56 in the picosecond to nanosecond time regime.

The next layer contains the L11δs, A60β, and F38. A60β has the highest S_{axis}^2 value of 0.79 in α_3D. The methyl groups of L11 show more dynamic S_{axis}^2 values relative to the methyl groups of L56 that pack to the left of it (Figure 7). Moreover, the δ methyl groups of I35 and I63 that pack next to the A60β layer show increased dynamics (Figure 7). A60 is the sole alanine residue and smallest side chain in the hydrophobic core of α_3D. The dynamic behavior around this region suggests that it may not have been the ideal residue for this position. Furthermore, the replacement of A60 with leucine or isoleucine increases the thermodynamic stability by 1.8 to 1.5 kcal mol^{-1} ($\Delta\Delta G_u$) relative to the wild-type α_3D (unpublished results). $^3J_{\alpha\beta}$, $^3J_{N\beta}$, $^3J_{C\delta C\alpha}$ coupling constants, and ^{1}H-^{1}H NOEs indicate that both the χ^1 and χ^2 angles of L11 undergo rotamer averaging, which may also contribute to the low S_{axis}^2 value. On the other hand, the $^3J_{\alpha\beta}$, $^3J_{N\beta}$

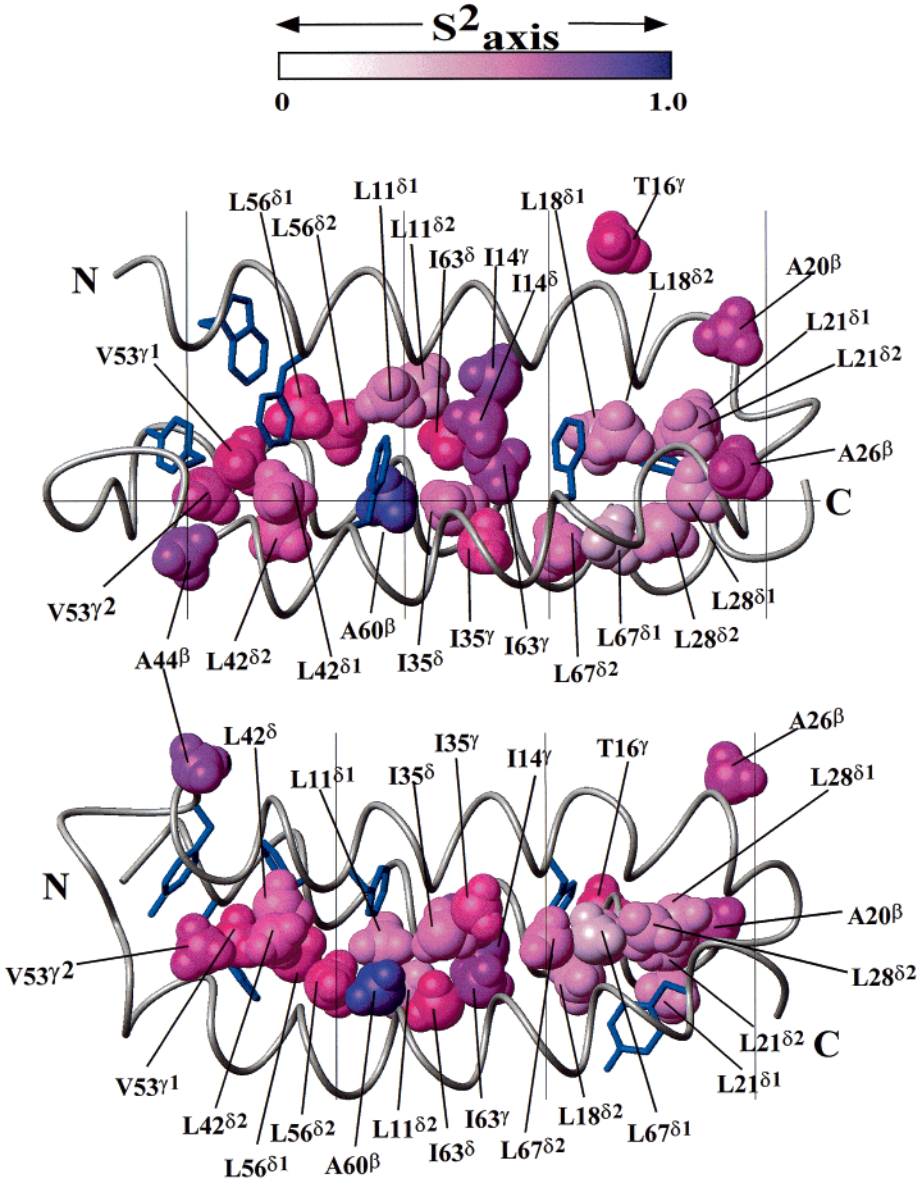

FIGURE 7: Color-coded representation of the S_{axis}^2 (^{2}H, SMF) values mapped onto the individual methyl groups of the solution structure of α_3D (PDB code 2A3D). The S_{axis}^2 values are coded from white (value of 0) to violet (value of 1) as depicted by the color scale. The aromatic side chains of W4, F7, F31, F38, Y45, and Y70 are labeled and shown as blue sticks. The figure was prepared with the program MolMol (*58*).

coupling constants, and ^{1}H-^{1}H NOEs show that F31 adopts the preferential χ^1 angle of $-60°$ (*12*, *53*).

The isoleucine layer of I14, I35, and I63 (the center of α_3D) shows a rigid environment with smaller S_{axis}^2 values for the δ methyl groups (I35δ and I63δ) that pack close to the A60β layer (Figure 7). The rigidified isoleucine layer may be attributed to the preference of the isoleucine side chain to adopt one rotamer state in an α-helix (*53*). Indeed, the $^3J_{\alpha\beta}$, $^3J_{N\beta}$, $^3J_{C\delta C\alpha}$ coupling constants, and ^{1}H-^{1}H NOEs indicate the preferred χ^1 and χ^2 angles for an α-helix of $-60°$ and 180°, respectively, for I14, I35, and I63 (*12*, *53*).

The C-terminal end of α_3D contains the hydrophobic layers with the most dynamic methyl groups in α_3D (Figure 7). The C-terminal end contains all leucine residues with two aromatic residues F31 and Y70 (Figure 7). The C-terminus of α_3D contains dynamic residues at both the backbone (Figure 1a) and side-chain level (Figure 3). The dynamic behavior of the C-terminal residues, Y70 to H73, may offer an explanation to the dynamic behavior seen in the methyl groups of L21, L28, and L18 (Figure 6). The $^3J_{\alpha N}$ coupling constant indicates that the ϕ dihedral angle for A69 is the last residue in an α-helical conformation, with the remaining residues 70−73 in mixed or extended conformation. The $^3J_{\alpha\beta}$, $^3J_{N\beta}$, $^3J_{C\delta C\alpha}$ coupling constants and ^{1}H-^{1}H NOEs indicate that both the χ^1 and χ^2 angles (60° and 60°, respectively) for L67 are unfavorable for an α-helix (*53*).

Kay and co-workers, investigating the methyl side-chain dynamics of the free and bound states of the pLCC-γ SH2 domains, showed that several leucine residues with low S_{axis}^2 values also experience rotameric averaging, even with the leucine residues being completely buried in the core (*54*, *55*). In a repacked hydrophobic core variant of ubiquitin, Handel and co-workers have shown that there was a good correlation between the dynamic methyl groups and side chains in unfavorable or averaged rotamers (*50*, *51*). This recurring theme is now seen for α_3D where five of the seven

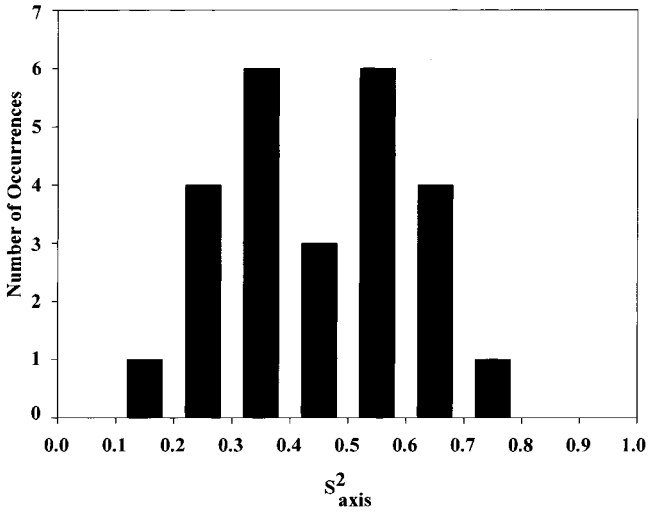

FIGURE 8: Histogram of the distribution of ^{2}H-derived S_{axis}^2 values obtained for the methyl groups of α_3D (see Table 2).

leucine residues have χ^2 angles undergoing rotamer averaging with the majority displaying low S_{axis}^2 values (Table 1). In contrast, all three isoleucine residues in α_3D adopt the preferential χ^1 and χ^2 angles for an α-helix (*53*), in addition to having high S_{axis}^2 values (Table 1 and Figure 6).

Implications for de novo Protein Design. Though it is now relatively straightforward to design protein sequences that adopt a desired secondary structural element, the design of large tertiary folds with well-defined hydrophobic cores remains a challenge (*56*). The reasons for this are only beginning to emerge. Site-resolved analysis of the main chain and side-chain dynamics may offer unique insights into the nature and therefore design of nativelike hydrophobic cores. From the NMR relaxation studies, α_3D has proven to be a successful design at the backbone level insofar as the backbone of the protein displays the dynamical properties of a native protein. The uniformly high squared generalized order parameters of the amide N−H and C_α-H support this view. Interestingly, however, certain features of the dynamics of methyl-bearing side chains of α_3D are distinct from that seen in studies of native state proteins and their complexes.

On average, the angular order of methyl-bearing side chains in α_3D is lower than that seen in natural proteins. Recently, Lee and Wand have suggested that a general feature of native proteins is the partitioning of subnanosecond motion of methyl bearing side chains into three classes of motion centered on S_{axis}^2 values of 0.3, 0.6, and 0.8 (*24*). Interestingly, α_3D also appears to have a nonuniform distribution of S_{axis}^2 values. Indeed, the two lower order classes appear to be represented in α_3D (Figure 8). Because of the effects of having only a limited number of samplings within the α_3D molecule it is difficult to discern a definitive distribution. Nevertheless, these data seem to suggest that α_3D is underrepresented in the most rigid class of methyl-bearing side chains seen in native proteins (*24*). Furthermore, the methyl rotation (τ_f) and methyl symmetry axis (τ_{axis}) time scales are larger than what has been observed for natural proteins.

There are lessons from the NMR relaxation studies of α_3D relating to the de novo design of proteins. One involves packing hydrophobic cores of proteins with several β-branched and aromatic amino acids and avoiding an overabundance of leucine residues. As observed in α_3D, aromatic residues apparently restrict the motion of methyl groups to adopt a conformationally specific hydrophobic core. Studies of de novo designed four-helix bundle proteins have also shown the benefits of packing cores with β-branched and aromatic amino acids (*3*, *5*, *57*). When packing hydrophobic cores using computational algorithms, potentially more weight should be given for rotamer preferences relative to optimizing for optimal van der Waals interactions.

CONCLUSIONS

The backbone and side-chain dynamics of α_3D, a de novo designed three-helix bundle protein, have been investigated. At the backbone level, both the ^{15}N−H and $^{13}C_\alpha$−H bond vectors display rigid motion in the α-helices of α_3D, with increasing motions at the ends of the α-helices and in the loop regions. Thus, the backbone dynamics of α_3D are similar to natural proteins. In contrast, methyl-bearing amino acids of α_3D display lower order than their counterparts in natural proteins. Additionally, the ^{13}C methyl data show that the methyl rotation rates (τ_f) to be more uniform and slightly longer than native proteins. The increased dynamics of the methyl groups of α_3D may be the consequence of several side chains switching between unfavorable or averaged rotamer states, thus reflecting rotameric strain in the hydrophobic core. Thus, the core of α_3D appears to have a higher degree of fluidity or malleability than natural proteins of similar size.

ACKNOWLEDGMENT

We thank Drs. Jeff Urbauer, Peter Flynn, and Blake Hill for helpful discussions and Dr. Brian Volkman for assistance in the data collection at NMRFAM.

REFERENCES

1. Bryson, J. W., Betz, S. F., Lu, H. S., Suich, D. J., Zhou, H. X., O'Neil, K. T., and DeGrado, W. F. (1995) *Science 270*, 935−941.
2. Lazar, G. A., and Handel, T. M. (1998) *Curr. Opin. Chem. Biol. 2*, 675−679.
3. Brive, L., Dolphin, G. T., and Baltzer, L. (1997) *J. Am. Chem. Soc. 119*, 8598−8607.
4. Bryson, J. W., Desjarlais, J. R., Handel, T. M., and DeGrado, W. F. (1998) *Protein Sci. 7*, 1404−1414.
5. Hill, R. B., and DeGrado, W. F. (1998). *J. Am. Chem. Soc. 120*, 1138−1145.
6. Johansson, J. S., Gibney, B. R., Skalicky, J. J., Wand, A. J., and Dutton, P. L. (1998) *J. Am. Chem. Soc. 120*, 3881−3886.
7. Baltzer, L. (1998) *Curr. Opin. Struct. Biol. 8*, 466−470.
8. Hill, R. B., Raleigh, D. P., Lombardi, A., and DeGrado, W. F. (2000) *Acc. Chem. Res. 33*, 745−754.
9. Imperiali, B., and Ottesen, J. J. (1999) *J. Pept. Res. 54*, 177−184.
10. Schafmeister, C. E., and Stroud, R. M. (1998) *Curr. Opin. Biotech. 9*, 350−353.
11. Street, A. G., and Mayo, S. L. (1999) *Struct. Folding Des. 7*, R105−R109.
12. Walsh, S. T. R., Cheng, H., Bryson, J. W., Roder, H., and DeGrado, W. F. (1999) *Proc. Natl. Acad. Sci. U.S.A. 96*, 5486−5491.
13. Kay, L. E., Torchia, D. A., and Bax A. (1989) *Biochemistry 28*, 8972−8979.
14. Schneider, D. M., Dellwo, M. J., and Wand, A. J. (1992) *Biochemistry 31*, 3645−3652.

15. Stone, M. J., Fairbrother W. J., Palmer, A. G., III., Reizer, J., Saier, M. H., Jr., and Wright, P. E. (1992) *Biochemistry 31*, 4394−4406.
16. Peng, J. W., and Wagner, G. (1992) *Biochemistry 31*, 8571−8586.
17. Nicholson, L. K., Kay, L. E., Baldisseri, D. M., Arango, J., Young, P. E., Bax, A., and Torchia, D. A. (1992) *Biochemistry 31*, 5253−5263.
18. Wand, A. J., Urbauer, J. L., McEvoy, R. P., and Bieber, R. J. (1996) *Biochemistry 35*, 6116−6125.
19. Le Master, D. M. (1999) *J. Am. Chem. Soc. 121*, 1726−1742.
20. Constantine, K. L., Friedrichs, M. S., Wittekind, M., Jamil, H., Chu, C.-H., Parker, R. A., Goldfarb, V., Mueller, L., II, and B. T. F. (1998). *Biochemistry 37*, 7965−7980.
21. Lee, A. L., Flynn, P. F., and Wand, A. J. (1999) *J. Am. Chem. Soc. 121*, 2891−2902.
22. Mittermaier, A., Kay, L. E., and Forman-Kay, J. D. (1999) *J. Biomol. NMR 13*, 181−185.
23. Lee, A. L., Kinnear, S. A., and Wand, A. J. (2000) *Nat. Struct. Biol. 7*, 72−77.
24. Lee, A. L., and Wand, A. J. (2001) *Nature 411*, 501−504.
25. Li, Z., Raychaudhuri, S., and Wand, A. J. (1996) *Protein Sci. 5*, 2647−2650.
26. Lee, A. L., Urbauer, J. L., and Wand, A. J. (1997) *J. Biomol. NMR 9*, 437−440.
27. Raiford, D. S., Fisk, C. L., and Becker, E. D. (1979) *Anal. Chem. 51*, 2050−2051.
28. Farrow, N. A., Muhandiram, R., Singer, A. U., Pascal, S. M., Kay, C. M., Gish, G., Shoelson, S. E., Pawson, T., Forman-Kay, J. D., and Kay, L. E. (1994) *Biochemistry 33*, 5984−6003.
29. Muhandiram, D. R., Yamazaki, T., Sykes, B. D., and Kay, L. E. (1995) *J. Am. Chem. Soc. 117*, 11536−11544.
30. Piotto, M., Saudek, V., and Sklenar, V. (1992) *J. Biomol. NMR 2*, 661−665.
31. Press, W. H., Teukolsky, S. A., Vetterling, W. T., and Flannery, B. P. (1992) *Numerical recipes in fortran 77: the art of scientific computing*, 2nd ed., Cambridge University Press, Cambridge.
32. Lee, L. K., Rance, M., Chazin, W. J., and Palmer, A. G., III (1997) *J. Biomol. NMR 9*, 94−100.
33. Lee, A. L., and Wand, A. J. (1999) *J. Biomol. NMR 13*, 101−112.
34. Lipari, G., and Szabo, A. (1982) *J. Am. Chem. Soc. 104*, 4546−4559.
35. Lipari, G., and Szabo, A. (1982) *J. Am. Chem. Soc. 104*, 4559−4570.
36. Clore, G. M., Szabo, A., Bax, A., Kay, L. E., Driscoll, P. C., and Gronenborn, A. M. (1990) *J. Am. Chem. Soc. 112*, 2989−2991.
37. Kroenke, C. D., Rance, M., and Palmer, A. G., III (1999) *J. Am. Chem. Soc. 121*, 10119−10125.
38. Ottiger, M., Tjandra, N., and Bax, A. (1997) *J. Am. Chem. Soc. 119*, 9825−9830.
39. Spiess, H. W. (1978) *NMR: Basic Principles and Progress 15*, 55−214.
40. Henry, E. R., and Szabo, A. J. (1985) *J. Chem. Phys. 82*, 4753−4761.
41. Mantsch, H. H., Saito, H., Smith, I. C. P. (1977) *Prog. NMR Spectrosc. 11*, 211−271.
42. Grzesiek, S., Vuister, G. W., and Bax, A. (1993) *J. Biomol. NMR 3*, 487−493.
43. Vuister, G. W., Wang, A., and Bax, A. (1993) *J. Am. Chem. Soc. 115*, 5334−5335.
44. Bax, A., Delaglio, F., Grzesiek, S., and Vuister, G. W. (1994) *J. Biomol. NMR 4*, 787−797.
45. Blackledge, M., Cordier, F., Dosset, P., and Marion, D. (1996) *J. Am. Chem. Soc.* 120, 4338−4339.
46. Dellwo, M. J., and Wand, A. J. (1989) *J. Am. Chem. Soc. 111*, 4571−4578.
47. Guenneugues, M., Drevet, P., Pinkasfeld, S., Gilquin, B., Menez, A., and Zinn-Justin, S. (1997) *Biochemistry 36*, 16097−16108.
48. Guenneugues, M., Gilquin, B., Wolff, N., Menez, A., and Zinn-Justin, S. (1999) *J. Biomol. NMR 14*, 47−66.
49. Fadel, A. R., Jin, D. Q., Montelione, G. T., and Levy, R. M. (1995) *J. Biomol. NMR 6*, 221−226.
50. Johnson, E. C., and Handel, T. M. (1999) *J. Biomol. NMR 15*, 135−143.
51. Johnson, E. C., Lazar, G. A., Desjarlais, J. R., and Handel, T. M. (1999) *Structure 7*, 967−976.
52. Hattori, A., Crespi, H. L., and Katz, J. J. (1965) *Biochemistry 4*, 1213−1225.
53. Stapley, B. J., and Doig, A. J. (1997) *J. Mol. Biol. 272*, 456−464.
54. Kay, L. E., Muhandiram, D. R., Farrow, N. A., Aubin, Y., and Forman-Kay, J. D. (1996) *Biochemistry 35*, 361−368.
55. Kay, L. E., Muhanddiram, D. R., Wolf, G., Shoelson, S. E., and Forman-Kay, J. D. (1998) *Nat. Struct. Biol. 5*, 156−163.
56. DeGrado, W. F., Summa, C. M., Pavone, V., Nastri, F., and Lombardi, A. (1999) *Annu. Rev. Biochem. 68*, 779−819.
57. Dolphin, G. T., Brive, L., Johansson, G., and Balter, L. (1996) *J. Am. Chem. Soc. 118*, 11297−11298.
58. Koradi, R., Billeter, M., and Wüthrich, K. (1996) *J. Mol. Graphics 14*, 51−55.

BI0105274